Journal of Applied Polymer Science

Strong and ductile poly(butylene adipate-*co*-terephthalate) biocomposites fabricated by oscillation shear injection molding

Xu-Juan Li,[1] Jing-Bin Chen,[1] Huan Xu,[1] Lan Xie,[1] Gan Ji Zhong,[1] Rong Ran,[1] Xu Ji,[2] Zhong-Ming Li[1]

[1]College of Polymer Science and Engineering, State Key Laboratory of Polymer Materials Engineering, Sichuan University, Chengdu Sichuan, 610065, People's Republic of China

[2]College of Chemical Engineering, Sichuan University, Chengdu Sichuan, 610065, People's Republic of China

Correspondence to: G.-J. Zhong (E-mail: ganji.zhong@scu.edu.cn), R. Ran (E-mail: ranrong@scu.edu.cn) and X. Ji (E-mail: jxhhpb@163.com)

ABSTRACT: Poor interfacial properties and uncontrollable phase morphology encountered during the fabrication of poly(butylene adipate-co-terephthalate) (PBAT)/thermal plastic starch (TPS) biocomposites, result unfortunately in low mechanical performances and thus limit its applications. Here an approach in terms of phase morphology controlling, i.e., extrusion compounding followed by oscillation shear injection molding (OSIM), is proposed to construct *in situ* TPS fiber and skin-core structure consisting of TPS fiber and droplet in skin layer, and spherical TPS in core layer, which tremendously benefits the mechanical properties. Specifically, the tensile strength, modulus and ductility for the biocomposites with various loadings of TPS, even when TPS loading as high as 55 wt %, outperform pure PBAT sample fabricated by conventional injection molding (CIM) with the increment of 51%, 308% in strength and modulus, respectively. Meanwhile, the elongation at breakage can maintain at 196%. The unprecedented establishment of high-performance PBAT/TPS biocomposites is in great need for potential applications, such as green packaging. © 2015 Wiley Periodicals, Inc. J. Appl. Polym. Sci. **2016**, *133*, 43312.

KEYWORDS: biopolymers and renewable polymers; composites; morphology; mechanical properties; structure–property relations

Received 20 July 2015; accepted 3 December 2015

DOI: 10.1002/app.43312

INTRODUCTION

Considerable efforts have been devoted to the development of the biodegradable polymers due to the urgent environmental concerns and the requirement of sustainable society.[1–5] With the merits of flexibility, desirable ductility, high use temperature, as well as good hydrophilicity and processing properties, poly(butylene adipate-*co*-terephthalate) (PBAT) has recently received increasing attention from both the academia and industry.[6–8] Unfortunately, the drawbacks, such as high production cost, low tensile strength, and uncontrollable degradability rate have limited its introduction in the market, where it is used as an optional alternative to replace the conventional nondegradable polyolefins in application of packing, agricultural mulch, etc.[9–12]

Native starch is a renewable and degradable carbohydrate, originating from various botanical sources. It is composed of linear polysaccharide molecules (amylose) and highly branched molecules, two types of polysaccharide based on α-D-glucose monomeric units.[13] In view of its low cost, overwhelming abundance, ongoing annual renewal and biodegradability in water and soil, incorporation of starch or thermoplastic starch (TPS) into polymer is considered as a promising approach to achieve high performance composites or even to fabricate fully biodegradable composites. Extensive studies have been conducted in its composite systems containing polyethylene,[14–20] such as low density polyethylene (LDPE),[21] linear low density polyethylene (LLDPE),[22] and biodegradable polyesters, poly(ε-caprolactone) (PCL),[23,24] polylactic acid,[25] PBAT,[26] poly(butylene succinate-*co*-adipate),[27] and poly(hydroxy ester ether),[28] etc. Although, the addition of TPS into polymer is expected to reach a combination of mechanical properties, biodegradability, low cost, and processability, which has a great potential to replace polyethylene products in packing application. However, compared to neat polymer, the mechanical properties of these composites usually decrease dramatically as TPS content increasing due to immiscible and incompatible nature between TPS and conventional polymers caused by high interfacial tension or phase aggregation. The tensile properties of LDPE and LLDPE blends containing TPS, as reported by Pieere *et al.*, showed that the modulus of the blends decreased with the increase of TPS content.[16] Koenig and Huang have investigated the mechanical properties of high amylose and waxy starch granules reinforced PCL biocomposites.[29,30] It was found that the elongation at break was the property most adversely

affected by the presence of TPS particles, it became brittle with the addition of 20–30 wt % TPS, which is attributed to inherent incompatibility. Similar observations based on wheat thermoplastic starch were obtained. As an example of PBAT/TPS system, the tensile strength sharply fell down to 17% of neat PBAT.[31] Thereby, achieving low-cost PBAT/TPS biocomposites with desirably mechanical properties are essential to the penetration of these materials into markets for various end use applications, such as packaging and transportation materials.[32–36]

It is pertinent to point out that the traditional approaches toward improving the properties of immiscible TPS/polymer composites are normally characterized by formulating[14,26] and associating with compatibilizers,[31,37] e.g., polyethylene-co-vinylalcohol,[38] polyethylene-co-acrylicacid,[19] polyethylene-co-glycidylmethacrylate,[39] polyethylene-g-maleicanhydride,[19] adipic acid,[29] and PBAT-*g*-maleicanhydride.[40] The results showed that through controlling of formulation, TPS/PE can acquire tensile strength, modulus and elongation at break of 83%, 108% and 83% of that of neat PE, respectively. For PBAT, improvement of mechanical properties by compatibilization was very limited, even in the best case, PBAT suffered from 50% of decrease in tensile strength. Therefore, it is still an ongoing challenge to improve the mechanical properties of PBAT/TPS biocomposite to obtain high performance, especially at high TPS content.

It has been established that for immiscible polymer blends, their performance not only depends on their components, but also highly on the phase interface and phase morphology, both of which are closely associated with the processing. High performance polymer composites can be obtained through the manipulating of morphology. Favis *et al.* demonstrated a balance of strength and elongation at break of TPS/PE blends at a great extent through obtaining TPS fiber by application of extension flow.[16,41] Li *et al.* manipulated the morphology of polyethylene terephthalate (PET) composites to obtain high performance goods owing to the formation of PET in-situ fiber,[42] furthermore, they successfully manipulated mechanical properties, conductive property of conductive polymer blends by controlling its morphology and phase structure.[43,44] Hence, there is a clear scientific and practical imperative requiring the control of phase morphology of the immiscible blends, aiming at the desirable balance of mechanical properties. In this study, we attempt to acquire high performance of PBAT/TPS biocomposites through controlling phase morphology and structure by incorporation of intensive shear flow and TPS content during the manufacturing of biocomposites. We adopted a special apparatus called oscillation shear injection molding (OSIM)[45,46] to control and manipulate the morphology of PBAT biocomposites, and investigated the influence of morphology on the mechanical properties of PBAT/TPS biocmoposites. Compared with conventional injection molding (CIM), OSIM increases two pistons, which can move reciprocally during injection packing stage to exert intensive shear stress on polymer melt to orient molecular chains, and to reduce viscosity of polymer. Consequently, enhancement of mechanical properties was obtained resulting from the orientation of molecular chains, modified morphologies such as shish-kebab,[47] transcrystallites,[48] *in situ* microfibrils[49] and fine dispersion of disperse phase.[50] It is believed that our exploration toward a rich fundamental understanding on the formation of shear-induced TPS in-situ microfiber, will extend the application of superior biodegradable PBAT/TPS production.

EXPERIMENTAL

Materials

Native corn starch was obtained from Huaxi Starch Company, Chengdu, China, which consists of 25 wt % amylose and 75 wt % amylopectin. Thermogravimetric Analysis (TGA) measurement showed that the water content in the starch granules was 9.1 wt %. Commercial poly(butylene adipate-*co*-butylene terephthalate) (melt flow index is 0.7 g/min, 190°C, 2.16 kg; Weight-average molecular weight is 0.7×10^5 g/mol) was kindly supplied by Blue Bridge Tunhe Polyester, China. The content of the butylene terephthalate unit of this sample was determined to be 47 mol %. The glycerol and citric acid (CA) all with 99.5% purity were used as a plasticizer.

Preparation of PBAT/TPS Composites

To avoid degradation and prevent formation of voids during processing, PBAT and native starch were dried at 80°C in vacuum oven overnight prior to extrusion or injection molding, respectively. TPS was prepared by the following procedures, the ratio of dry starch to glycerol and citric acid was 100/40/1 phr (by weight) in all cases. 1 phr (w/w, dry basis) of CA was dissolved into 40 phr glycerol to form homogeneous solvent, then 100 phr native starches were added, mixed, and dried in an oven at 60°C for 12 h to obtain TPS.

PBAT/TPS biocomposites were fabricated in a corotating twin screw extruder (Nanjing Keya Machinery Plant, China) with a ratio of screw length to its diameter (*L/D*) of 40. Temperatures in six zones were set at 95, 130, 145, 145, 140, 130°C from feed section to metering section, respectively, and the screw speed was held constantly at 150 rpm. To decrease the cost of PBAT/TPS biocomposites, we focus on the mechanical improvement of PBAT/TPS with high TPS content. Here, three types of biocomposites have difference in the PBAT/TPS ratios of 70/30, 55/45, 45/55 by weight, respectively.

The extruded pellets of the biocomposites after drying were injection molded into standard dumbbell test samples, the barrel temperature profiles were set at 115, 150, 150, 150, and 155°C from hopper to nozzle, respectively. During packing stage, a controlled shear flow was continuously imposed on the melt by pistons using OSIM technology, which has two hydraulically actuated pistons that move reciprocally at the same frequency of 0.3 Hz and the pressure of 13 MPa. The cycle time of the sample preparation by OSIM and CIM was fixed at 3 min in this study. CIM samples were also prepared under the same processing condition (only without oscillatory shear) for comparison, designated as C of each formula, for instance, C30, C45, and C55 represent PBAT/TPS in the weight ratios of 70/30, 55/45, and 45/55 under CIM condition respectively, whereas under OSIM condition that was designated as O in the same way, such as O30, O45, and O55, respectively. Neat PBAT molded by CIM and OSIM was designated as Nc and No, respectively.

Scanning Electron Microscopy (SEM)

SEM was employed to observe the phase structure of the injection molded parts. Cryogenic fracture was applied to obtain the

specific surfaces. For the cryogenic fracture, the injection molded samples were placed in liquid nitrogen for 0.5 h, finally the samples were cryogenically fractured along the shear flow direction (i.e., molding direction). A field-emission SEM (Inspect F, FEI, Finland) was utilized to explore the phase morphology of the composite samples sputter-coated with gold, while the accelerated voltage was held at 20 kV.

Differential Scanning Calorimetry (DSC)

DSC traces were recorded using a DSC Q2000 calorimeter under a nitrogen atmosphere for a sample weight of 5–8 mg at a heating rate of 10°C/min from −60 to 180°C, to examine the thermal behavior of the PBAT/TPS. The T_g values were defined as the midpoint of the heat capacity change while crystallization and melting temperature were defined as the maxima of the DSC peaks. Using eq. (1), the crystallinity of all samples was estimated according to the enthalpy obtained from the DSC curves.

$$X_C^{DSC}=(\Delta H_m)/(\Delta H_0)x\times 100 \quad (1)$$

where corresponding enthalpy changes, ΔH_m is melting enthalpy, and, the melting enthalpy for 100% crystallized PBAT is 114 J/g,[51] x is the weight fraction of PBAT in the corresponding biocomposites.

To investigate the effect of TPS on PBAT crystallization process, the non-isothermal crystallization of PBAT/TPS was conducted at a cooling rate of 20°C/min. Crystallization temperature (T_m) is defined as the midpoint of the heat capacity change, while half-time of crystallization ($t_{1/2}$) was obtained from the time at which the relative crystallization degree (X_t) of samples reached 50%. X_t was calculated according to the following equation[52]:

$$X_t=\frac{Q_t}{Q_\infty}=\frac{\int_0^t (dH/dt)dt}{\int_0^\infty (dH/dt)dt} \quad (2)$$

where Q_t and Q_∞ are the heat generated at time (t) and infinite time, respectively, and dH/dt is the rate of heat evolution.

Two-Dimensional Wide-Angle X-ray Diffraction (2D-WAXD)

2D-WAXD determination was employed to evaluate molecular orientation and crystalline morphology of PBAT/TPS biocomposites at the beamline BL15U1 of SSRF, Shanghai. The monochromated X-ray beam with a wavelength of 0.124 nm was focused to an area of 3 × 2.7 μm^2 (length × width), and the distance from sample to detector was set as 185 mm. The 2D-WAXD images were collected with an X-ray CCD detector (Model SX165, Rayonix, USA).

The orientations of the crystals of PBAT were calculated using the Hermans orientation parameter, which is defined as

$$<P2(\cos\phi)>=(3<\cos^2\phi>-1)/2 \quad (3)$$

in which $<\cos^2\phi>$ is an orientation factor defined as

$$<\cos^2\phi>=\int_0^{\frac{\pi}{2}} I(\phi)\cos^2\phi\sin\phi d\phi \Big/ \int_0^{\frac{\pi}{2}} I(\phi)\sin\phi d\phi \quad (4)$$

where $I(\phi)$ is the scattering intensity at ϕ. The orientation parameter has a value of unity when all the crystals are oriented with their c axes parallel to the reference direction, a value of −0.5 when all the c axes are perpendicular to the reference direction, and a value of 0 with totally random orientation. For our samples, the orientation parameter was calculated mathematically using Picken's method from the (010) reflection of WAXD for PBAT.[42]

Mechanical Properties Tests

Tensile properties of the dumbbell samples were measured at room temperature using the Instron Instrument Model 5576 according to ASTM D 638 at a cross-head speed of 100 mm/min. A minimum of 6 bars for each sample were tested at the same condition, and the average values were presented with standard deviation.

Dynamic Mechanical Analysis (DMA)

DMA experiments, performed on a Q800 DMA from TA instruments, were conducted on rectangular bars of PBAT/TPS (dimensions of length × width × thickness are 40 mm × 6 mm × 4 mm) obtained from the middle zone of injection-molded specimens. The specimens were tested in a multi frequency strain mode with a dual cantilever bending mode at a frequency of 1 Hz with a target amplitude of 25 mm. The scanning rate was set at 3°C/min in the range of −100 to 80°C. Storage modulus (E') and loss tangent ($\tan\delta$) were recorded as a function of temperature. The thermal transitions were determined from the maxima of the tan δ peaks.

The interfacial interaction parameter between fillers and polymer matrix can also be evaluated by the following equation[53]:

$$\tan\delta=\tan\delta_m/(1+1.5B\Phi) \quad (5)$$

where $\tan\delta$ and $\tan\delta_m$ are the loss tangent of filled polymer composites and unfilled polymers, respectively; represents the volume fraction of the fillers; B is an interaction parameter, a quantitative measurement of interfacial adhesion between filler and polymer matrix. A large value of B means a better interaction between the two phases.

Fourier Transform Infrared Spectrophotometry (FTIR)

Attenuated total reflectance Fourier transform infrared (ATR-FTIR) spectra were performed using a Nicolet 6700 spectrometer (Thermal Scientific, USA) set at a 2 cm^{-1} resolution, from wave number of 4000 cm^{-1} to 650 cm^{-1} to measure the occurrence of esterification reaction.

RESULTS AND DISCUSSION

Shear Flow Induced Structures in PBAT/TPS Biocomposites

Phase Morphology of PBAT Biocomposite. SEM micrographs of PBAT biocomposites are shown in Figure 1. For comparison, the micrographs of CIM samples are also shown in Figure 1(a–c), in which the average diameter of TPS disperse phase increases dramatically from ~0.1 μm [Figure 1(a)] to ~5 μm [Figure 1(b)] when content of TPS reaches 45 wt %, probably resulting from the agglomeration of TPS. With further increasing TPS concentration to 55 wt %, it is difficult to distinguish matrix from the dispersed phase that it maybe form cocontinuous phase due to phase conversion. Avérous *et al.* found that the percolation threshold of PBAT/TPS composites can be as low as 25 wt %.[54] Additionally, from core to skin zone, homogeneous phase morphology is observed in CIM samples.

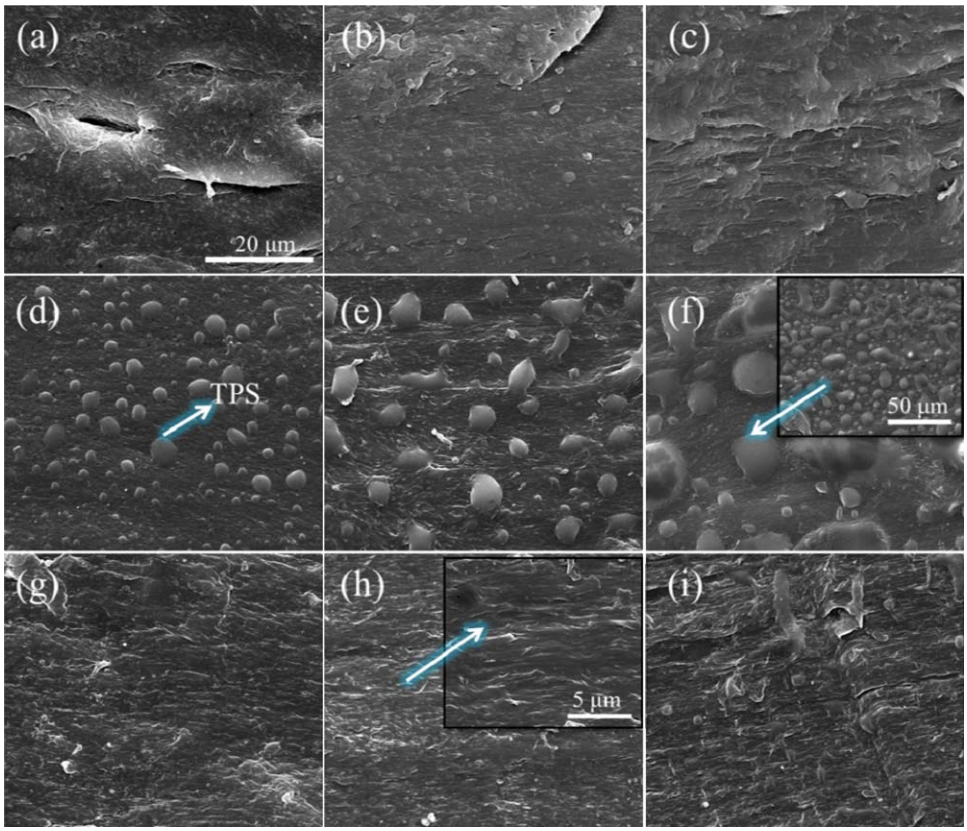

Figure 1. SEM images of cryofractured surfaces of PBAT/TPS biocomposites fabricated by CIM and OSIM techniques. (a) C30; (b) C45; (c) C55; (d), (e), (f) represent phase morphology in core layer of O30, O45, and O55; The inserted picture in (f) shows a bigger area of sample. (g), (h), and (i) are the corresponding phase morphology in skin layer of O30, O45, and O55, respectively; The inserted picture in (h) represents corresponding local magnified area. [Color figure can be viewed in the online issue, which is available at wileyonlinelibrary.com.]

For OSIM samples, two different phase morphologies can be clearly observed in core layer and skin layer (i.e., skin-core structure). In core layer, TPS presents spherical dispersed phase [shown in Figure 1(d–f)], which is due to the relaxation of deformed TPS at weaker shear stress and higher temperature, compared to skin layer. The average diameter of TPS moderately increases to 2.5 μm for O45 and rushes to 10 μm for O55, compared to the lowest value of 2.2 μm in O30. The increment of TPS size suggests that there is an agglomeration with increasing of TPS content. While in skin layer, fibril-like TPS is observed [shown in Figure 1(g–i)]. In Figure 1(h), the TPS fiber with a diameter of 0.2 μm can be seen, suggesting that shear stress in OSIM processing leads to the change of TPS morphology. The condition of the formation of TPS fiber is different from the results obtained by Favis *et al.*,[41] who found that TPS fibers could be obtained when the amount of the glycerol exceeded 29 wt % using one-step single-twin screw extruder with slit die. In our case, the formation of fibers results primarily from the application of oscillatory shear flow during injection molding, when the glycerol is 28 wt %. The morphology transition may be triggered by the flow field in different processing method. Therefore, intensive shear flow under OSIM technology also can be used to manipulate phase morphology and to construct different PBAT biocomposties phase structure coupling with TPS loading.

Crystalline Structure and Molecular Orientation of PBAT Composites. Crystallinity, crystal polymorphism and molecular orientation are closely related to the mechanical properties of the composites based on the semi-crystalline polymer matrix. WAXD was performed to acquire such information of PBAT/TPS biocomposites prepared by CIM and OSIM techniques. Figure 2 shows 2D-WAXD patterns of CIM and OSIM samples of PBAT biocomposties with various TPS contents. The three distinct diffractions of all samples in the WAXD patterns represent the (010), (−111), and (100) crystal planes of PBAT, respectively. The arc-like diffractions in Figure 2(a) for OSIM samples evidently imply the orientation of PBAT crystals. To reveal the orientation degree of the PBAT molecular chains, the (010) intensity distribution along the azimuthal angle between 0 and 360° was integrated and shown in Figure 2(b). It shows that the orientation degree decreases with increasing TPS content, but only O45 with much stronger signal can be calculated the orientation parameter of 0.749. By contrast, the orientation parameters of other samples cannot accurately be calculated due to their weak intensities. However, orientation degree of OSIM is clearly higher than the corresponding CIM samples. Meanwhile, the crystallinity as shown in Table I indicates that incorporation of TPS significantly increases the crystallinity of PBAT/TPS biocomposites due to nucleating effect. The slight lower crystallinity of OSIM than CIM samples may be due to the

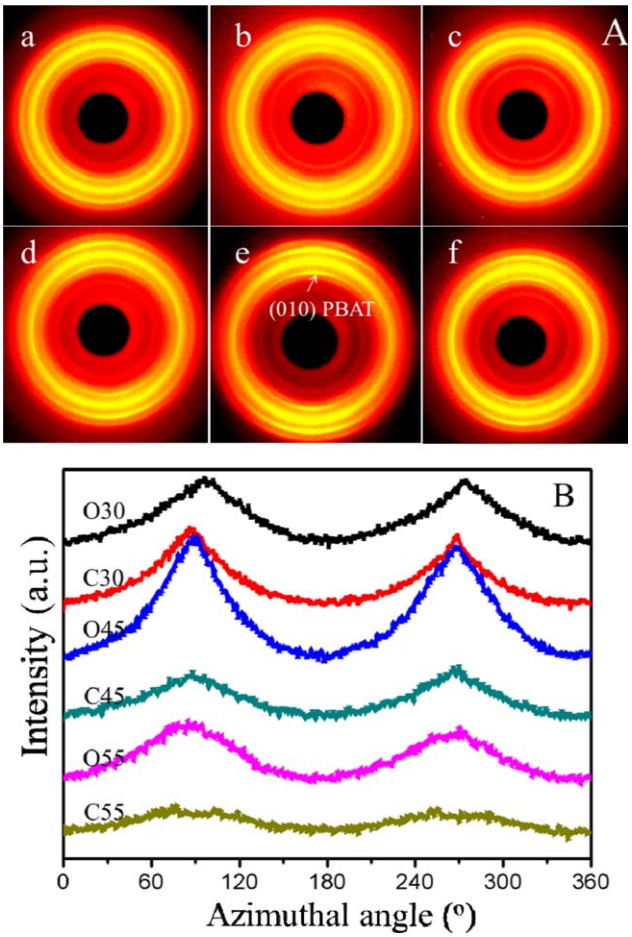

Figure 2. 2D-WAXD patterns of PBAT biocomposites fabricated by CIM and OSIM techniques. (A) 2D patterns of PBAT/TPS biocomposites. (a) C30; (b) C45; (c) C55; and (d) O30; (e) O45; (f) O55; (B) (010) azimuthal distribution of PBAT/TPS biocomposites. [Color figure can be viewed in the online issue, which is available at wileyonlinelibrary.com.]

different morphology and particle size of TPS in OSIM and CIM samples. Since TPS acts as nucleation agent, its nucleation ability should be partly affected by its morphologies and sizes, finally resulting in the slight difference of crystallinity. To identify the polymorphism and crystallinity of PBAT/TPS biocmoposites, 1D-WAXD curves of samples were measured and plotted in Figure 3. Four diffraction peaks located at 2θ angles of 17.3°, 20.2°, 23.1°, and 25.0° are related to basal reflections (010), (−111), (100), and (11-1), respectively,[55] which shows a triclinic crystal system, the same crystal structure as pure PBAT. These results indicate that intensive shear flow can increase orientation of PBAT molecules without variation of crystal polymorphism.

Thermal Behavior of PBAT Biocomposites

Thermal Behavior of PBAT Biocomposites by DSC. Heating traces of PBAT and its biocomposites under CIM and OSIM condition are plotted in Figure 4. The corresponding parameters, such as melting temperature (T_m), melting enthalpy (ΔH_m), and crystallinity (X_c), are listed in Table II. As seen, for both CIM and OSIM samples, there is an evident decrease in T_m of all PBAT/TPS

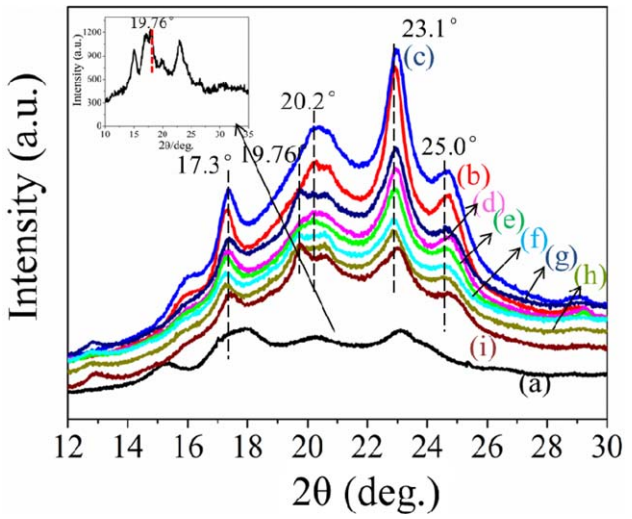

Figure 3. 1D-WAXD curves of PBAT biocomposites. (a) native starch; (b) Nc; (c) No; (d) C30; (e) O30; (f) C45; (g) O45; (h) C55; and (i) O55. The inserted picture is the magnified curves of native starch. [Color figure can be viewed in the online issue, which is available at wileyonlinelibrary.com.]

biocomposites, compared to that of neat PBAT, which suggests that the introduction of TPS leads to the formation of relatively imperfect lamellae of PBAT. In addition, T_m values for OSIM samples are slightly higher than that of CIM samples. It is unexpected that X_c values increase with TPS loading increasing in all biocomposites. The significantly increased X_c of PBAT biocomposites suggests that TPS can act as nucleating agent and can accelerate the crystallization rate of PBAT in all biocomposites. Such nucleating effect of TPS on PBAT is similar to that of polylactic acid (PLA),[56,57] LLDPE,[58] high density polyethylene,[59] PCL,[60] and poly(1,4-dioxan-2-one) (PPDO).[61]

To confirm the nucleation of TPS, non-isothermal crystallization of PBAT/TPS biocomposites at a cooling rate of 20°C/min was performed by DSC. The onset crystallization temperature (T_{onset}), peak crystallization temperature (T_{peak}) and crystallization enthalpy (ΔH_c) for the biocomposites are presented for comparison and the half-time of crystallization ($t_{1/2}$) is evaluated. T_{onset} of C55 improves about 4°C (from 73.81°C for neat PBAT to 77.92°C for C55 in Figure 5), calculated $t_{1/2}$ decreases from 1.40 min to 0.93 min, which confirms that the TPS exactly acts as a nucleation agent to accelerate crystallization rate of PBAT in the biocomposites.

Dynamic Mechanical Properties of PBAT and Its Biocomposites. Storage modulus is an indicator of the elastic properties and loss tangent is regarded as a damping factor

Table I. Details of Crystallinities and Orientation Parameters of Samples under CIM and OSIM Condition

	O30	C30	O45	C45	O55	C55
X_c (%)	31.24	32.98	32.87	35.27	42.31	45.90
Orientation parameter	–	–	0.749	–	–	–

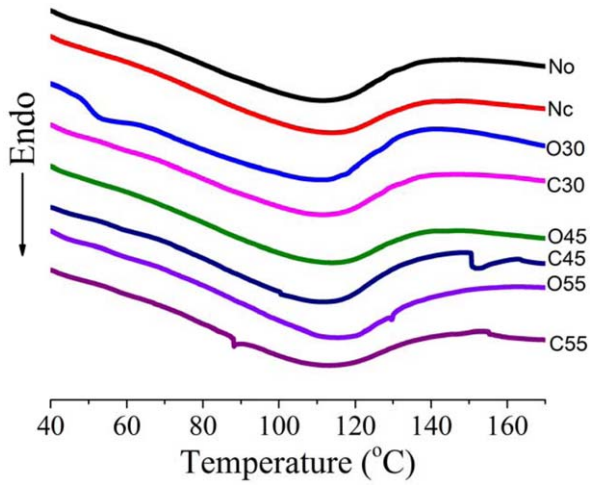

Figure 4. The DSC curves of PBAT biocomposites molded by CIM and OSIM. [Color figure can be viewed in the online issue, which is available at wileyonlinelibrary.com.]

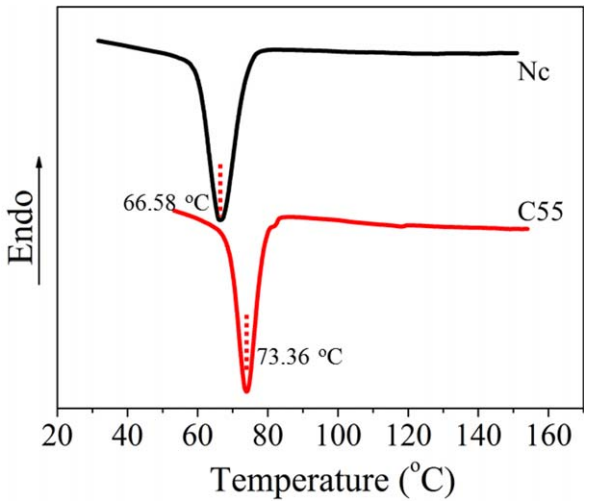

Figure 5. Nonisothermal crystallizaiton of PBAT and its biocomposites at a cooling rate of 20°C/min. [Color figure can be viewed in the online issue, which is available at wileyonlinelibrary.com.]

which is very sensitive to any phase transformation. The glass transition is generally defined as the temperature at which the loss tangent rises up to its maximum value. The storage modulus and loss tangents of PBAT/TPS biocomposites as a function of temperature are shown in Figure 6. Apparently, storage modulus is affected by the addition of TPS. Neat PBAT displays a major damping peak at −14°C associated with a drastic drop in storage modulus (E'). Below T_g, the storage modulus of biocomposites is lower than that of neat PBAT except samples with 30 wt % TPS and exhibits two transitions with increase of temperature, which suggests that there are more than one phase structure in biocomposites. Above T_g, because the modulus of TPS is in the range of hundreds of MPa,[62,63] much higher than that of PBAT, therefore, PBAT/TPS biocomposties are similar to filler filled polymer systems,[64] storage moduli of them are higher than that of neat PBAT. Furthermore, it is interesting to observe that the storage moduli of CIM samples are higher than that of OSIM samples. This improvement may be ascribed to the sphercial shape dispersed TPS in PBAT matrix under CIM condition and stronger interface between PBAT and TPS, which is also consistent with the enhancement in stiffness.

The phase structure and interfacial interaction of PBAT/TPS biocomposites were investigated from loss tangent in Figure 6(b). Evolution of tan δ versus temperature mainly shows three transitions. The middle temperature (around −14°C) corresponds to the glass transition of PBAT (Table III).

Table II. Effects of Composition and Shear on T_m, ΔH_m, and X_c of PBAT Biocomposites

Sample	T_m (°C)	ΔH_m (J/g)	X_c (%)
O-30	112.29	18.94	23.73
C-30	110.06	21.23	26.60
O-45	111.78	16.92	27.13
C-45	110.86	20.46	32.63
O-55	111.64	19.48	37.97
C-55	108.81	21.49	41.89
No	116.26	10.62	9.31
Nc	115.07	10.56	9.26

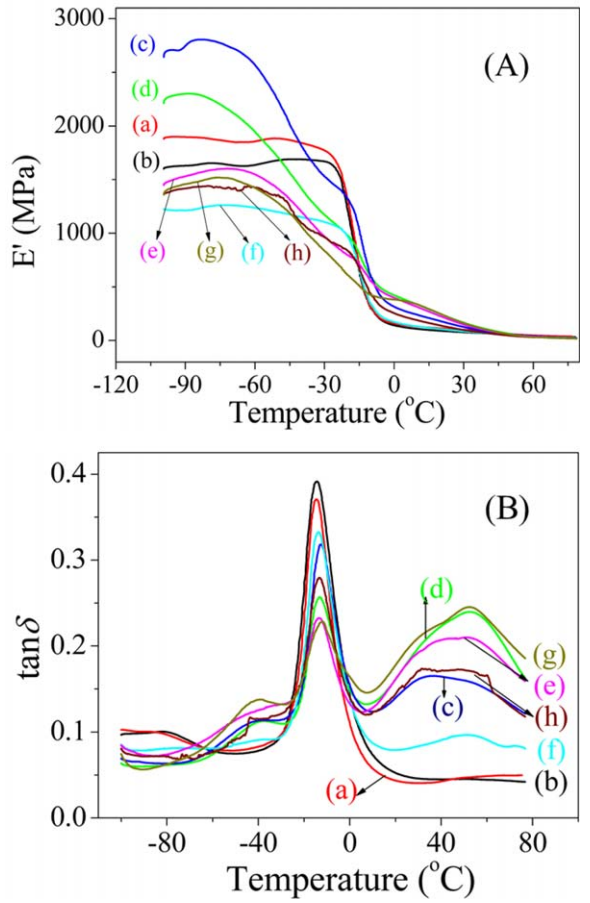

Figure 6. (A) Storage modulus and (B) Loss tangent as a function of the temperature for PBAT biocomposites. (a) Nc, (b) No, (c) C30, (d) O30, (e) C45, (f) O45, (g) C55, and (h) O55. [Color figure can be viewed in the online issue, which is available at wileyonlinelibrary.com.]

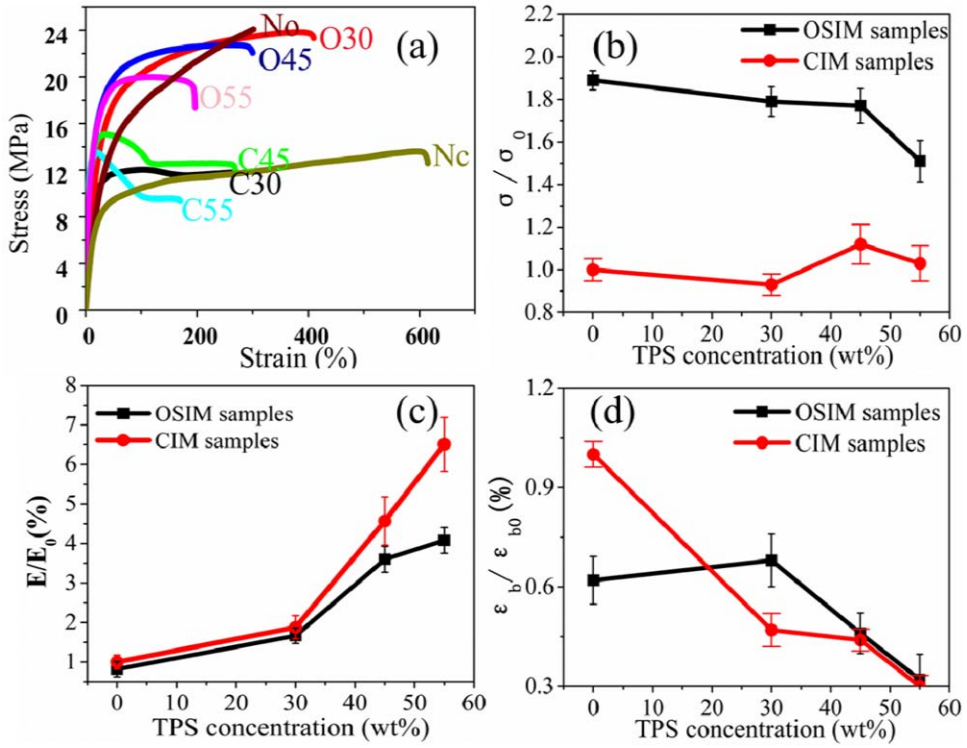

Figure 7. (a) Stress−strain curves, (b) Relative stress strength, (c) Relative Young's modulus (E/E_0) and (d) Relative elongation at break ($\varepsilon_b/\varepsilon_{b0}$) of PBAT biocomposits as a function of TPS concentration (wt %). Terms with subscript 0 refer to the pure PBAT. [Color figure can be viewed in the online issue, which is available at wileyonlinelibrary.com.]

Incorporation of TPS in matrix, T_g of PBAT shifts up to −11°C, which indicates an enhancement of interfacial adhesion between the TPS and PBAT. Meanwhile, it suggests that the movement of PBAT chains is impeded when in the presence of TPS. The interfacial interaction parameters between TPS and PBAT are evaluated from Figure 6(b) by eq. (5) and listed in Table IV. The values of B of all biocomposites are positive, which confirms a relatively high physical interaction between PBAT and TPS. The B values of all OSIM samples, except samples with 30 wt % TPS, are lower than that of CIM samples, which indicates that the enhanced compatibilty is achieved in CIM samples. This result is in agreement with SEM observation and the change of storage modulus, finally results in an increment of mechanical properties shown in Figure 7. The stronger interaction could be ascribed to the special partial esterification on the external surface of TPS,[65] corresponding to the redshift of C—O in C—O—C and C═O in ester bond as shown in Figure 8.

Besides the changes of T_g transition, the two other transitions in Figure 6 are assigned to the TPS phase. For glycerol contents higher than 10–15 wt %, as described by Lourdin *et al.*,[66,67] a relaxation peak can be found at low temperature, close to the glass transition of glycerol, suggesting that a phase separation (glycerol demixing) occurs in thermoplastic starch. This peak corresponds to a glycerol rich phase β transition.[66]

For all the PBAT biocomposites, a tan δ peak located around −55°C is observed [Table III, Figure 6(b)]. For the binary blends, this peak represents the secondary relaxation of starch and corresponds to the secondary-transition of glycerol-rich domains. Lourdin *et al.*[68] and Averous *et al.*[23] observed that tan δ peak for the β transition was strongly dependent on glycerol content. The similar results were observed by Favis *et al.*,[69] furthermore, they found that the TPS concentration in blend had no effect on starch plasticization. In this article, we reveal some unexpected transition behaviors. The T_β transition of OSIM sample is strongly dependent on TPS content at constant glycerol concentration and shear flow. With increasing of TPS, T_β value of CIM is constant around −43°C, on the contrary, that of OSIM decreases gradually, which is possibly due to the formation of TPS fiber to enhance the diffusion of glycerol and leads to further phase separation. Finally, increasing TPS content could result in large size of free glycerol phase after phase separation.

The other transition, α relaxation, can be ascribed to the glass transition of the starch-rich phase (Table III). As for various amounts of TPS and different processing methods, T_α values are found to be higher than room temperature, consequently, the TPS phase in the biocomposites should demonstrate a glass behavior for all PBAT biocomposites. Because the modulus of starch-rich phase is much higher than that of PBAT and TPS is in the glass state in the testing temperature range, similar to filler filled polymer system[55]; therefore, storage modulus of the PBAT biocomposites is significantly higher than that of neat PBAT and increases with TPS content when temperature is above T_g. The variation trend of T_α is similar to that of T_β. T_α

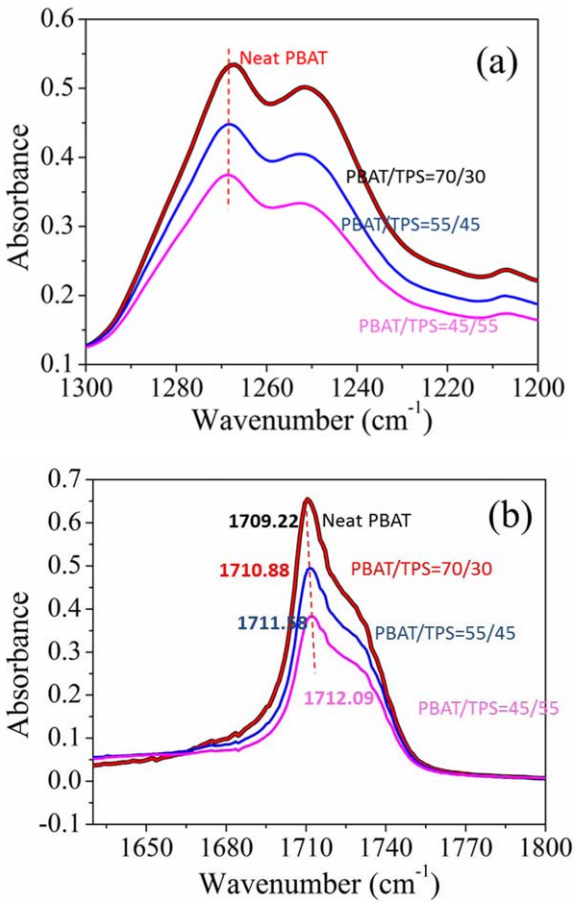

Figure 8. The FTIR spectrum of PBAT/TPS biocomposites. (a) C—O in C—O—C; (b) C═O in ester bond. [Color figure can be viewed in the online issue, which is available at wileyonlinelibrary.com.]

value of OSIM samples maintains around 50°C, while that of CIM samples increases from 36.30 to 52.28°C. This phenomena may be due to the morphology of spherical TPS homogenously dispersed in CIM samples, when increasing of TPS, it is equal to reduction of glycerol content. The different variation trend of T_α and T_β of PBAT biocomposites uner OSIM and CIM condition implies that oscillatory shear in OSIM process can generate unique structure and aid mechanical property improvement shown in Figure 7.

The results of DMA indicate that the TPS content and shear have a positive effect on starch plasticization to control the phase structure (as shown in Figure 1), enhancing the mobility

Table III. Interaction Parameters Evaluated from tan δ

Sample	Loss tangent	Interaction parameter (B)
No	0.3915	/
Nc	0.3610	/
O30	0.2510	3.86
C30	0.3181	0.93
O45	0.3229	0.83
C45	0.2261	2.34
O55	0.2750	1.21
C55	0.2237	1.75

of molecules and the compatibility between TPS and PBAT. Through controlling TPS content and shear flow, manipulation of phase structure can be realized to obtain different properties.

Tensile Mechanical Properties

Stress-Strain Behavior. The tensile properties of a polymer blend strongly depend on its composition, interfacial adhesion and morphologies. The stress strain curves of the biocomposites [Figure 7(a)] show a typical tensile behavior of polymer blends or composites composed of a rigid dispersed phase in a soft matrix with good interfacial adhesion. The notable difference is that CIM samples have a yield point, whereas OSIM samples do not have. The OSIM stress-strain curves are similar to those of neat PBAT, which suggests that besides compatibility, crystallinity and orientation, there must be another special morphology in OSIM samples. This morphology is conducive to stress transfer and finally leads to the enhancement of mechanical properties.

Ultimate Tensile Strength (σ_{max}). The ultimate tensile strength (σ_{max}) of PBAT biocomposites (defined as the highest stress during drawing) is shown in Figure 7(b). PBAT biocomposites maintain a high percentage of the ultimate tensile strength of pure PBAT (σ_{max}/σ_0) even at high TPS loading. σ_{max} values of PBAT biocomposites containing 55 and 45 wt % TPS, whether prepared by CIM or OSIM, are even higher than that of pure PBAT under CIM condition. It is interesting to observe that for OSIM samples, the ultimate tensile strength is even nearly double than that of CIM samples. It is well known that the mechanical properties of blends are closely related to the phase morphology, the shape of filler, the compatibility between polymer and filler, crystallinity, orientation of molecules etc. In our case, OSIM samples with TPS loading below 45 wt % have better σ values, which is may due to high orientation of molecules

Table IV. Transition Temperatures Measured from tan δ

TPS concentration (wt %)	T_g of PBAT (°C)		T_β (°C)		T_α (°C)	
	O	C	O	C	O	C
0	−14.29	−13.14	/	/	/	/
30	−11.66	−12.51	−39.05	−43.96	51.96	36.30
45	−12.24	−11.68	−54.19	−44.46	52.24	42.66
55	−11.74	−10.67	−65.22	−41.68	50.73	52.28

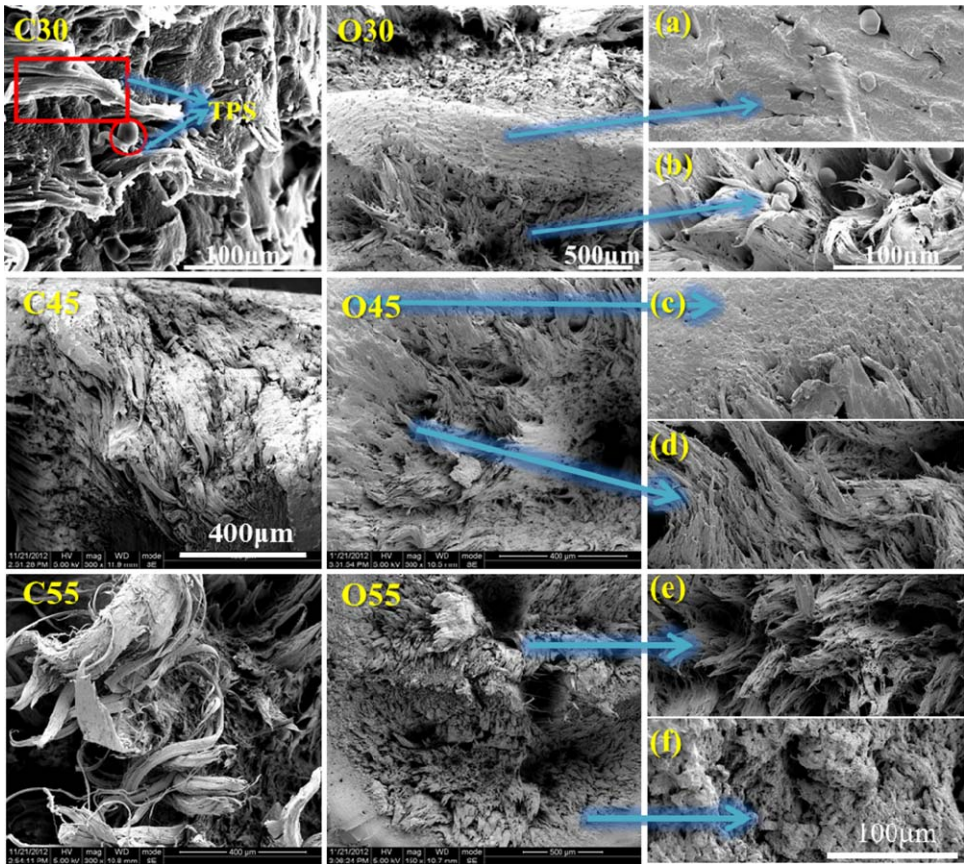

Figure 9. Morphology of PBAT biocomposites after failure, (a) and (b), the magnified images of skin and core layer in O30 sample respectively; (c) and (d), the corresponding images of O45; (e) and (f), the corresponding images of O55. [Color figure can be viewed in the online issue, which is available at wileyonlinelibrary.com.]

induced by shear flow. However, at high TPS loading, excellent σ value of OSIM samples of low orientation degree may be attributed to compact long in-situ TPS fiber induced by oscillatory shear flow.

Young's Modulus. The relative Young's modulus (E/E_0) is depicted in Figure 7(c). Once again the performances of OSIM samples stands out. Young's modulus (E) can be maintained at high levels even at high loading of TPS. In cases of both CIM and OSIM biocomposites, the E of PBAT/TPS biocomposites, beyond that of pure PBAT, improves gradually with increasing of TPS loading. The result is similar to that of PE/TPS, whose E is higher than that of pure PE when the glycerol content is 29 wt %.[53] These results are ascribed to the high E value of starch rich phase in glass state at testing temperature. When glycerol content in TPS is lower than 30 wt %, the spherical dispersed TPS in biocomposites will be difficult to deform and behaves like rigid filler. Consequently, the more the TPS content is, the higher the E of composites. Meanwhile, an interesting phenomenon can be seen that the E of OSIM biocomposites is lower than that of CIM samples, which is consistent with DMA results shown in Figure 6, which should be further investigated for clarity.

Elongation at Break (ε_b). The relative elongation at break ($\varepsilon_b/\varepsilon_{b0}$) in the machine direction of PBAT/TPS biocomposites was shown in Figure 7(d). The results are also excellent and demonstrate that at high TPS loading (55 wt %), the ε_b of biocomposites is near 200%, which is much higher than that of reported.[70] The ε_b value of PBAT biocomposite drops with increasing of the TPS concentration. Meanwhile, although shear stress from OSIM could lead to molecular orientation and formation of TPS fibrils, which could deteriorate the elongation at break, the values of OSIM biocomposites are comparable to that of CIM samples. The enhanced properties may be attributed to the water removal in partially and the ability of TPS phase to deform. The presence of water at the processing temperature (150°C) can lead to the formation of bubbles in the extrudate, which weakens the final product. In this work, the native starch (9.1 wt % water) was dried at 80°C for 12 h under vacuum oven to make sure the water is less than 1 wt % before mixing with PBAT. On the other hand, the researchers found that fibrillar TPS was facilitate to improve ε_b[42] we also assume that the ability of TPS phase to deform is mainly attributed to maintenance of ε_b. DMA result shows that OSIM samples have lower transition temperature than that of CIM samples; therefore, when subjected to the external stress, the TPS in OSIM is apt to deform and maintain higher elongation.

Phase Morphology after Tensile Failure. To interpret the effect of shear and TPS content on phase structure, the SEM micrographs after tensile failure were investigated and shown in

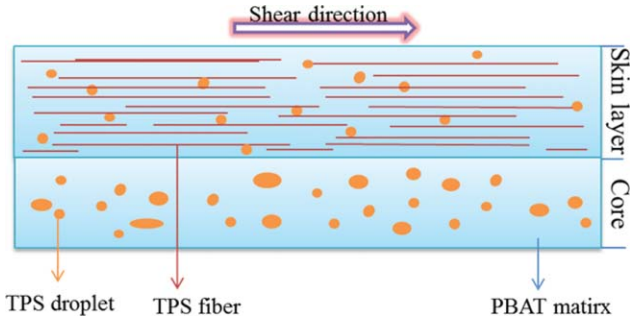

Figure 10. Schematic of skin-core structure of PBAT/TPS biocomposites. [Color figure can be viewed in the online issue, which is available at wileyonlinelibrary.com.]

Figure 9. It is interesting that the phase morphology in OSIM is very different from that of CIM samples. In C30 of Figure 9, TPS in form of fiber and droplet disperses in PBAT matrix, like sea-island structure in a typical polymer composites. Whereas, in skin layer of O30, O45, and O55 samples shown in Figure 9(a,c,d), TPS presents fibril-like, which results from intensive shear stress and lower temperature to induce the deformation and orientation of TPS. As for core layer [Figure 9(b,d,e)], TPS is spherical or irregular droplet possibly caused by relaxation and weak shear stress. According to Figures 1 and 9, schematic of skin-core structure of PBAT/TPS biocomposites was drawn and shown in Figure 10. Fibril-like co-continuous phase, enhanced orientation degree of PBAT and the deformability of TPS improve the elongation at break of PBAT/TPS, consequently, the biocomposites can maintain high strength and ductility. Therefore, OSIM technology represents a very effective approach to tailor the mechanical properties of PBAT biocomposites, and finally to obtain a promising balance of modulus, tensile strength, and elongation at breakage by the formation of different phase morphology.

The formation of skin-core phase structure may be due to two factors, the first one is the difference in viscosity between starch-rich phase and glycerol-rich phase; the second one is oscillatory shear flow. Unlike in CIM process, in OSIM process, intensive oscillatory shear was imposed on samples to reduce the viscosity of starch, glycerol and PBAT and to orient the molecular chain segment, consequently, glycerol-rich phase with lower viscosity firstly fills the mold surface to form *in situ* fiber, while relative high viscosity starch-rich phase stays in core layer and hardly deforms due to weak shear stress and relaxation.

CONCLUSIONS

This work reports on high performance of PBAT/TPS fabricated by OSIM technology. The OSIM sample of PBAT biocomposites demonstrates a high level of tensile strength beyond neat PBAT, meanwhile a good balance of ductility even at very high loading of TPS. The properties can be tailored using combination of both shear flow and TPS content to generate a sophisticated morphology. Results of DSC, WAXD, and DMA show that higher crystallinity, molecular orientation, and desirable interfacial interaction can enhance stiffness and tensile strength. Through a control of thermoplastic starch concentration, the classic sea-island structure can be seen in CIM process. By contrast, a novel phase morphology, called skin-core structure comprised of TPS fiber in skin layer and TPS droplet in core layer, can be achieved by OSIM technology. This unique morphology significantly improves the tensile strength and modulus of the biocomposites over neat PBAT even at high TPS loading, accompanied by a good balance of ductility.

ACKNOWLEDGMENTS

The authors are grateful for the financial supports from the National Natural Science Foundation of China (Grant Nos. 51120135002, 51421061, 51473101, and 51273131), the Doctoral Program of the Ministry of Education of China (Grant 20130181130012). We acknowledge the National Synchrotron Radiation Laboratory, Shanghai, China, for synchrotron WAXD measurements, and the fund from State Key Laboratory of Polymer Materials Engineering, China (sklpme 2014-3-08).

REFERENCES

1. Arvanitoyannis, I. S. *J. Macromol. Sci. Part C: Polym. Rev.* **1999**, *39*, 205.
2. Arvanitoyannis, I. S.; Nakayama, A.; Aiba, S. *Carbohydr. Polym.* **1998**, *36*, 105.
3. Yu, L.; Christie, G. *J. Mater. Sci.* **2005**, *40*, 111.
4. Dean, K.; Yu, L.; Wu, D. Y. *Compos. Sci. Technol.* **2007**, *67*, 413.
5. Liu, H.; Xie, F.; Yu, L.; Chen, L.; Li, L. *Prog. Polym. Sci.* **2009**, *34*, 1348.
6. Witt, U.; Einig, T.; Yamamoto, M.; Kleeberg, I.; Deckwer, W. D.; Müller, R. *J. Chemosphere* **2001**, *44*, 289.
7. Someya, Y.; Sugahara, Y.; Shibata, M. *J. Appl. Polym. Sci.* **2005**, *95*, 386.
8. Jiang, L.; Wolcott, M. P.; Zhang, J. W. *Biomacromolecules* **2006**, *7*, 199.
9. Siegenthaler, K. O; Künkel, A.; Skupin, G.; Yamamoto, M. In Synthetic Biodegradable Polymers; Rieger, B., Künkel, A., Coates, G. W., Reichardt, R., Dinjus, E., Zevaco, T. A., Eds.; Springer: Berlin Heidelberg, **2012**; Vol. *245*, p 91.
10. Prashantha, K.; Soulestin, J.; Lacrampe, M.; Krawczak, P. *Polym. Polym. Compos.* **2009**, *17*, 205.
11. Fukushima, K.; Wu, M. H.; Bocchini, S.; Rasyida, A.; Yang, M. C. *Mater. Sci. Eng. C: Mater. Biol. Appl.* **2012**, *32*, 1331.
12. Brodhagen, M.; Peyron, M.; Miles, C.; Inglis, D. A. *Appl. Microbiol. Biotechnol.* **2015**, *99*, 1039.
13. Zobel, H. *Starch-Stärke* **1988**, *40*, 44.
14. Lawrence, S. S.; Walia, P. S.; Felker, F.; Willett, J. L. *Polym. Eng. Sci.* **2004**, *44*, 1839.
15. Aburto, J.; Thiebaud, S.; Alric, I.; Borredon, E.; Bikiaris, D.; Prinos, J.; Panayiotou, C. *Carbohydr. Polym.* **1997**, *34*, 101.
16. St-Pierre, N.; Favis, B. D.; Ramsay, B. A.; Ramsay, J. A.; Verhoogt, H. *Polymer* **1997**, *38*, 647.
17. Bikiaris, D.; Prinos, J.; Panayiotou, C. *Polym. Degrad. Stab.* **1997**, *56*, 1.

18. Bikiaris, D.; Prinos, J.; Panayiotou, C. *Polym. Degrad. Stab.* **1997**, *58*, 215.
19. Bikiaris, D.; Prinos, J.; Koutsopoulos, K.; Vouroutzis, N.; Pavlidou, E.; Frangis, N.; Panayiotou, C. *Polym. Degrad. Stab.* **1998**, *59*, 287.
20. Prinos, J.; Bikiaris, D.; Theologidis, S.; Panayiotou, C. *Polym. Eng. Sci.* **1998**, *38*, 954.
21. Mortazavi, S.; Ghasemi, I.; Oromiehie, A. *Polym. Test.* **2013**, *32*, 482.
22. Wang, S. J.; Yu, J. G.; Yu, J. L. *Polym. Degrad. Stab.* **2005**, *87*, 395.
23. Averous, L.; Moro, L.; Dole, P.; Fringant, C. *Polymer* **2000**, *41*, 4157.
24. Wu, C. S. *Polym. Degrad. Stab.* **2003**, *80*, 127.
25. Wu, C. S. *Macromol. Biosci.* **2005**, *5*, 352.
26. Averous, L.; Fauconnier, N.; Moro, L.; Fringant, C. *J. Appl. Polym. Sci.* **2000**, *76*, 1117.
27. Yu, L.; Dean, K.; Yuan, Q.; Chen, L.; Zhang, X. M. *J. Appl. Polym. Sci.* **2007**, *103*, 812.
28. Zhou, G.; Willett, J. L.; Carriere, C. J.; Wu, Y. V. *J Polym. Environ.* **2000**, *8*, 145.
29. Koenig, M. F.; Huang, S. *J. Polymer* **1995**, *36*, 1877.
30. Huang, S. J.; Koenig, M. F.; Huang, M. In Biodegradable Polymers and Packaging; Ching, C. T. K., Kaplan, D. L., Thomas, E. L., Eds.; Technomic Publishing Company: Lancaster, PA, **1993**; p 97.
31. Raquez, J. M.; Nabar, Y.; Narayan, R.; Dubois, P. *Polym. Eng. Sci.* **2008**, *48*, 1747.
32. Reddy, N.; Yang, Y. *Biotechnol. Bioeng.* **2009**, *103*, 1016.
33. Pashkuleva, I.; Marques, A. P.; Vaz, F.; Reis, R. L. *J. Mater. Sci.-Mater. M* **2005**, *16*, 81.
34. Mano, J. F.; Koniarova, D.; Reis, R. L. *J. Mater. Sci.-Mater. M* **2003**, *14*, 127.
35. Lai, S. M.; Huang, C. K.; Shen, H. F. *J. Appl. Polym. Sci.* **2005**, *97*, 257.
36. Raquez, J. M.; Nabar, Y.; Narayan, R.; Dubois, P. *J. Appl. Polym. Sci.* **2011**, *122*, 639.
37. Silva, I. F. E.; Yamashita, F.; Mueller, C. M. O.; Mali, S.; Olivato, J. B.; Bilck, A. P.; Grossmann, M. V. E. *Int. J. Food. Sci. Tech.* **2013**, *48*, 1762.
38. Sailaja, R. R. N.; Chanda, M. *J. Appl. Polym. Sci.* **2002**, *86*, 3126.
39. Sailaja, R. R. N.; Reddy, A. P.; Chanda, M. *Polym. Int.* **2001**, *50*, 1352.
40. Maliger, R. B.; McGlashan, S. A.; Halley, P. J.; Matthew, L. G. *Polym. Eng. Sci.* **2006**, *46*, 248.
41. Rodriguez-Gonzalez, F. J.; Ramsay, B. A.; Favis, B. D. *Polymer* **2003**, *44*, 1517.
42. Picken, S. J.; Aerts, J.; Visser, R.; Northolt, M. G. *Macromolecules* **1990**, *23*, 3849.
43. Li, B.; Zhang, Y. C.; Li, Z. M.; Li, S. N.; Zhang, X. N. *J. Phys. Chem. B* **2009**, *114*, 689.
44. Pang, H.; Chen, T.; Zhang, G. M.; Zeng, B. Q.; Li, Z. M. *Mater. Lett.* **2010**, *64*, 2226.
45. Na, B.; Wang, Y.; Zhang, Q.; Fu, Q. *Polymer* **2004**, *45*, 6245.
46. Ibar, J. *Polym. Eng. Sci.* **1998**, *38*, 1.
47. Yang, H. R.; Lei, J.; Li, L.; Fu, Q.; Li, Z. M. *Macromolecules* **2012**, *45*, 6600.
48. Wang, K.; Guo, M.; Zhao, D. G.; Zhang, Q.; Du, R. N.; Fu, Q.; Dong, X.; Han, C. C. *Polymer* **2006**, *47*, 8374.
49. Zhong, G. J.; Li, L.; Mendes, E.; Byelov, D.; Fu, Q.; Li, Z. M. *Macromolecules* **2006**, *39*, 6771.
50. Wang, K.; Liang, S.; Du, R. N.; Zhang, Q.; Fu, Q. *Polymer* **2004**, *45*, 7953.
51. Mohanty, S.; Nayak, S. K. *Int. J. Plast. Technol.* **2009**, *13*, 163.
52. Feng, S. H.; Wu, D. F.; Liu, H. Y.; Chen, C.; Liu, J. L.; Yao, Z.; Xu, J.; Zhang, M. *Thermochim. Acta* **2014**, *587*, 72.
53. Zeng, S. S.; Reyes, C.; Liu, J. J.; Rodgers, P. A.; Wentworth, S. H.; Sun, L. *Polymer* **2014**, *55*, 6519.
54. Schwach, E.; Avérous, L. *Polym. Int.* **2004**, *53*, 2115.
55. Shi, X. Q.; Ito, H.; Kikutani, T. *Polymer* **2005**, *46*, 11442.
56. Cai, J.; Liu, M.; Wang, L.; Yao, K. H.; Li, S.; Xiong, H. G. *Carbohydr. Polym.* **2011**, *86*, 941.
57. Li, S.; Xiong, Z. Y.; Fei, P.; Cai, J.; Xiong, H. G.; Tan, J.; Yu, Y. *J. Appl. Polym. Sci.* **2013**, *129*, 3566.
58. Sabetzadeh, M.; Bagheri, R.; Masoomi, M. *Carbohydr. Polym.* **2015**, *119*, 126.
59. Kahar, A. W. M.; Ismail, H. *J. Vinyl. Addit. Techn.* **2014**, 1.
60. Cai, J.; Xiong, Z. Y.; Zhou, M.; Tan, J.; Zeng, F. B.; Ma, M. H.; Lin, S.; Xiong, H. G. *Carbohydr. Polym.* **2014**, *102*, 746.
61. Wang, X. L.; Yang, K. K.; Wang, Y. Z.; Wu, B.; Liu, Y.; Yang, B. *Polym. Degrad. Stab.* **2003**, *81*, 415.
62. Li, H. B.; Huneault, M. A. *J. Appl. Polym. Sci.* **2011**, *119*, 2439.
63. Boo-Young, S.; Sang-Ii, L.; Young-Sub, S.; Balakrishnan, S.; Narayan, R. *Polym. Eng. Sci.* **2004**, *44*, 1429.
64. Sumita, M.; Tsukihi, H.; Miyasaka, K.; Ishikawa, K. *J. Appl. Polym. Sci.* **1984**, *29*, 1523.
65. Shi, R.; Zhang, Z. Z.; Liu, Q. Y.; Han, Y. M.; Zhang, L. Q.; Chen, D. F.; Tian, W. *Carbohydr. Polym.* **2007**, *69*, 748.
66. Lourdin, D.; Bizot, H.; Colonna, P. *J. Appl. Polym. Sci.* **1997**, *63*, 1047.
67. Lourdin, D.; Coignard, L.; Bizot, H.; Colonna, P. *Polymer* **1997**, *38*, 5401.
68. Lourdin, D.; Bizot, H.; Colonna, P. *Macromol. Symp.* **1997**, *114*, 179.
69. Sarazin, P.; Li, G.; Orts, W. J.; Favis, B. D. *Polymer* **2008**, *49*, 599.
70. Chen, F.; Zhang, J. W. *Polymer* **2010**, *51*, 1812.